Chemistry

Physical & Theoretical Chemistry fields

Okayama University *Year* 2006

Properties of a novel hard-carbon optimized to large size Lion secondary battery studied by 7Li NMR

Kazuma Gotoh* Mariko Maeda† Aisaku Nagai‡
Atsushi Goto** Masataka Tansho†† Kenjiro Hashi‡‡
Tadashi Shimizu§ Hiroyuki Ishida¶

*Okayama University, kgotoh@cc.okayama-u.ac.jp
†Kureha Corporation
‡Kureha Corporation
**National Institute for Materials Science
††National Institute for Materials Science
‡‡National Institute for Materials Science
§National Institute for Materials Science
¶Okayama University

Properties of a novel hard-carbon optimized to large size Li ion secondary battery studied by ^{7}Li NMR

Kazuma Gotoh*[a], Mariko Maeda[b], Aisaku Nagai[b], Atsushi Goto[c], Masataka Tansho[c], Kenjiro Hashi[c], Tadashi Shimizu[c] and Hiroyuki Ishida[a]

[a] *Department of Chemistry, Faculty of Science, Okayama University, Okayama 700-8530, Japan*

[b] *Research Center, Kureha Corporation, Iwaki, Fukushima 974-8686, Japan*

[c] *National Institute for Materials Science, Tsukuba, Ibaraki 305-0003, Japan*

Abstract

The state of lithium in a novel hard-carbon optimized to the anode of large size Li ion secondary battery, which has been recently commercialized, was investigated and compared with other existing hard-carbon samples by ^{7}Li NMR method. The new carbon material showed a peak at 85 ppm with a shoulder signal at 7 ppm at room temperature in static NMR spectrum, and the former shifted to 210 ppm at 180 K. The latter at room temperature was attributed to Li doped in small particles contained in the sample. The new carbon sample showed weaker intensity of cluster-lithium signal than the other hard-carbon samples in NMR, which corresponded to a tendency of less "Constant Voltage" (CV) capacity in charge-discharge curves of electrochemical evaluation. Smaller CV capacity and initial irreversible

capacity, which are the features of the novel hard-carbon, are considered to correspond to a blockade of the diffusion of Li into pore of carbon.

Keywords: hard carbon; Lithium; battery; ^{7}Li NMR; anode; electric vehicle

***Corresponding author**. Tel.: +81 86 251 7776 ; fax: +81 86 251 7832

E-mail address: kgotoh@cc.okayama-u.ac.jp (K. Gotoh).

Introduction

Carbon has been used as an anode active material in lithium ion secondary batteries (LIB) [1]. One of the carbon materials, non-graphitizable carbon (hard-carbon), was used as an attractive anode in the early days of LIB used practically; however, in the present days graphite is mostly used as anode because LIB is mainly used to small size instruments that need high energy density per cell volume, for instance, portable PC, cellular phone, *etc*.

Recently, hard-carbon has been reconsidered as a prominent anode active material of LIB with increasing an expectation of application to large size instruments. Its properties of high power and long durability are expected to be superior as the power source of large size batteries [2], for example, the battery used to Pure Electric Vehicle (PEV) or Hybrid Electric Vehicle (HEV).

The structure and the electrochemical property of hard-carbon have been investigated by various methods. The existence of void (micropore) in hard-carbon has been implied from the smaller density of hard-carbon (≈1.5 g cm^{-3}) than graphite (2.26 g cm^{-3}) [3]. The pore is not thought to be connected easily to outer space because very slow adsorption of N_2 gas into hard-carbon for over 1 week is observed when the nitrogen adsorption isotherm is measured. Concerning the pore, some authors (Franklin [4], J. Conard et al.[5], and so on [6][7]) proposed the structure of hard-carbon.

It was reported that the lithium fully-doped in hard-carbon showed

a broad ^{7}Li NMR signal at about 85~120 ppm at room temperature [8][9][10][11][12][13][14][15]. Tatsumi et al. have shown that the signal for Li-doped no-graphitizable carbon splits to two peaks at 192 ppm and 18 ppm at 143 K [9]. The 192 ppm signal was explained by quasimetallic lithium forming a lithium cluster in the pore of hard-carbon structure. The 18 ppm peak was attributed to the Li ion intercalated into graphene layers and the Li ion existing on the edge of carbon.

One of characteristic properties of LIB using hard-carbon as anode is that the charge-discharge curve shows two stages, viz. the stage proportional to charge voltage and the stage of constant voltage (CV). The cell can be charged (lithiated) fast by constant current (CC) in the former stage, while in the CV stage it is charged slowly with keeping the potential at 0 V. The CV stage has been noticed as the origin of higher capacity than 372 mAh g^{-1} of theoretical graphite anode of LiC_6, however, it is not preferred for large size battery. The power sources of large instruments like electric vehicles require a high charge-discharge rate (10～40 C) [2], which can not be achieved at the CV stage of hard-carbon. On the other hand, the rate property of CC stage is generally superior to graphite. Still more, state of charge (SOC) of battery can be easily observed and controlled on the CC stage since it is proportional to the voltage of cell, and strong pulse-like input and output can be received because of the enough margin of electronic potential. Therefore, hard-carbon having little CV capacity is desired for large size battery. In general, heat treating of hard-carbon by high

temperature can result smaller CV capacity but also leads to smaller CC capacity.

Recently, a novel hard-carbon having low CV capacity, Carbotron P(J) (Kureha Corporation), has been supplied. This carbon is expected to be good for large size battery because of smaller initial irreversible capacity and CC capacity same as normal hard-carbon. We intended to investigate the properties of the new carbon comparing the normal hard-carbons, Carbotron PS(F) and Carbotron P(F) (Kureha Corporation), and to make clear the state of lithium doped in the hard-carbon by ^{7}Li NMR method.

Experimental

The hard-carbon samples, (A), (B) and (C) are Carbotron P(J), Carbotron PS(F) and Carbotron P(F), respectively, which are prepared from a petroleum pitch and heat-treated in non-reactive gases [16][17]. The SEM observation on the surface of (A) is shown in Fig. 1. X-ray powder diffraction (XRD) patterns of three samples were measured on Rigaku RAD-C diffractometer with roter-flex and Cu-K_{α} radiation. The particle sizes of samples were measured on Micromeritics Microtrac-FRA laser diffraction particle size analyzer.

Test cells using carbon samples as anode active materials were made to evaluate the electrochemical properties as well as to obtain the specimens for NMR measurements. Lithium metal was employed as a

counter electrode. The electrolyte of 1 mol dm^{-3} $LiPF_6$ solution in 1:1 (volume ratio) propylene carbonate (PC):dimethyl carbonate (DMC) was used. Electrochemical lithium insertion was performed at first with constant current (CC) density of 0.5 mA cm^{-2}. After the cell voltage reached to 0.0 V, the cell was kept at 0.0 V until the equilibrium current (the CV lithiation process). Electrochemical lithium extraction process carried out galvanostatically at 0.5 mA cm^{-2}.

The lithiated carbon electrodes were taken out from the cells and washed by DMC in an Ar atmosphere. After drying, the specimens were sealed into sample tubes with He gas for MAS NMR and static NMR measurements. ^{7}Li MAS NMR spectra were recorded on sample (A) to observe the dependence of insertion capacity by Bruker AVANCE 400 spectrometer at room temperature. The spinning rate was 5 kHz. Three spectra at the cell voltage of 0.1 V (155 mAh g^{-1}; the end of the CC lithiation process), 0.0 V (300 mAh g^{-1}; fully lithiation), and 0.0 V (500 mAh g^{-1}; the end of the CV lithiation process) were measured. Static ^{7}Li NMR measurements were performed by 11.7 T magnet and Thamway spectrometer at the temperatures between 30 and 293 K. The signal of saturated LiCl water solution was used as the 0 ppm-standard for the ^{7}Li NMR chemical shift above 273 K for both NMR measurements. Below 273 K, the center of the signal of LiCl powder was defined as 0 ppm. A single pulse sequence was adopted to the measurements.

Results

XRD and particle size analyses

XRD patterns of three samples are shown in Fig. 2. The interlayer distances and the crystallite size factors (L_c) calculated from XRD(002) reflection using Scherrer formula [18] are given in Table 1. The particle size distributions of (A), (B) and (C) are illustrated in Fig. 3. The average particle sizes estimated from distributions are shown in Table 1. The average size of (C) is larger than (A) and (B).

Electrochemical evaluation

Charge-discharge curves of cells using the hard-carbon samples, (A), (B) and (C), are shown in Fig. 4. The capacities of CC stage, CV stage and initial irreversible capacity are shown in Table 2. The capacity of 305 mAh g^{-1} on CC stage in (A) was larger than that of 264 mAh g^{-1} in (B) and 240 mAh g^{-1} in (C), while CV stage capacity in (A) (47 mAh g^{-1}) was quite smaller than that of 266 mAh g^{-1} in (B) and 271 mAh g^{-1} in (C). On the other hand, (B) and (C) showed similar properties except the smaller initial irreversible capacity of (C).

^{7}Li NMR spectra

Fig. 5 shows ^{7}Li MAS NMR spectra on the anode active material (A). At 0.1 V, two peaks at 9.4 ppm and 0.5 ppm were observed. The former peak shifted and split into two components at 54.4 ppm and about 15 ppm at

0.0 V (300 mAh g^{-1}; fully lithiation). The spectrum at 0.0 V (500 mAh g^{-1}; the end of the CV lithiation process) consisted of three components: a wide component at 91.9 ppm, a small signal of 0.5 ppm and the shoulder structure about 15 ppm. In addition, the signal of deposited Li metal at 263 ppm [19] was observed in the 0.0 V (500 mAh g^{-1}) spectrum.

Static ^{7}Li NMR spectrum of sample (A) showed a peak at 85 ppm with a shoulder signal at 7 ppm at room temperature (Fig. 6). The signal of 7 ppm did not shift while the intensity changed somewhat depending on temperature. The shape and the width of the signal hardly changed below 150 K except the increasing of the intensity by low temperature effect below 30 K. On the other hand, the peak of 85 ppm shifted gradually with broadening and became to 210 ppm at 180 K. The signal broadened further and disappeared below 120 K. The spectrum of sample (B) showed three peaks at 10, 106 and 265 ppm at room temperature (Fig. 7). The peak of 265 ppm corresponding to the shift of Li metal was not observed below 270 K. The peaks of 10 and 106 ppm behaved similar to sample (A), however, the ratio of the intensities of two peaks was different. For example, the intensity of 10 ppm contrasted with 106 ppm at 180 K on (B) is smaller than that of 7 ppm with 85 ppm on (A). In the case of (C), only a peak of 109 ppm was observed at room temperature (Fig. 8). It split into two peaks of 15 and 198 ppm at 180 K, and the latter disappeared, in the same manner as (A) and (B).

Discussion

The splitting of a peak below 240 K in Li NMR spectra of hard-carbon has been reported by some authors [9][11][12][13][14][15]. According to their analysis, as for sample (A) ~ (C), the static NMR signals of 85-106 ppm at room temperature are explainable by contribution of rapid exchange of two sites: Li ion in graphene layers and quasimetallic Li cluster in pores. The signal of 7-15 ppm observed in (A) and (B) at room temperature can be attributed to Li ion in an environment similar to graphene layers and exchanging to other sites slower than NMR time scale ($\approx 10^{-9}$ s).

Effects on particle size of samples

Anode materials (A) and (B) have almost same particle size distributions and (C) has larger particles than (A) and (B) (Fig. 3 and Table 1). Especially, no particles smaller than 2 μm are involved in (C) while a few particles in (A) and (B) have the diameters below 2 μm. Therefore, the origin of 7-15 ppm shift at room temperature in (A) and (B) is attributable to the small particles in anode active material. To confirm this, ^{7}Li MAS NMR (Fig. 9) was measured for sample (B) and a refined sample (D) which was made by sieving and cutting off over 5 μm particles of (B) (shown the particle size in Fig. 3). The sieved sample showed three asymmetric peaks: 118 ppm corresponding to 106 ppm of the static NMR spectrum of (B) (Fig. 7), and 65

ppm attributable to quasimetallic Li, and 0.6 ppm with a shoulder structure about 10-20 ppm. Although it is lower than 7 ppm, the last peak (0.6 ppm) can be attributed to 7-15 ppm shift of static NMR (Fig. 7) because the peak is considered to have strong anisotropy since the sidebands of the peak is apparent. The peak and shoulder structure of 0.6 ppm are also observed in (B) (Fig. 9 i)), however, the intensities are quite smaller than the signal of Li cluster at 120 ppm. From the existence of quasimetallic Li peak at 65 ppm and the comparison of the intensities of the peaks, it is supposed that the environment of Li intercalated in small particles below 2 μm contained in anode active material is different from that in larger hard-carbon particles. It is inferred that some small particles have few pores, and Li in the particles don't exchange between inner graphene and pores.

Generally, anode active materials having smaller particle sizes are preferred because a coating process of electrode become more easily and an anode of LIB can be thinner. Moreover, it is expected that larger surface area leads stronger output of LIB, which is especially hoped in the case of large size devices. Therefore, the behavior of Li in small particles contained in hard-carbon is not negligible and will be taken care more in near future.

Comparison of the structure and the property of carbon (A) and (B)

From MAS NMR result, it seems that at first Li is doped on the edge of graphene and intercalated into graphene layers, then Li creates cluster structure in pores as soon as graphene layers filled with Li ion. According

to the above process, it is expected that the capacity of the CC stage and CV stage on charge-discharge curves (Fig. 4) correspond to the NMR signals of Li in graphene layers and Li cluster, respectively. The static NMR spectra of sample (A) and (B) at 180 K could be deconvoluted to two components (Fig. 10) which can be belonged to inner layer and cluster, although the signal might have other components different minutely, for instance, 0.6 ppm peak with the shoulder structure in MAS NMR spectra (Fig. 5, 9). The reasons adopted the 180 K spectra are as follows: 1) Spectra above 210 K can be deconvoluted to over three components. It may begin spectra-narrowing above 210 K. 2) Below 150 K the signal of Li cluster weakened as cutting off the head of the short time FID. The ratio of cluster Li signal to inner-layer Li signals on each sample (A) and (B) is evaluated to be 0.26 and 1.17, respectively. It is estimated from NMR results that the cluster Li exists in sample (B) about 4.5 (= 1.17 / 0.26) times of sample (A). On the other hand, the ratios of CV capacity / CC capacity on (A) and (B) are evaluated to 0.15 (= 47 / 305) and 1.00 (= 266 / 264), respectively. This difference shows the fact that Li cluster is formed before CV process, i.e., quasimetallic lithium is born at the potential higher than 0 V, which has also been suggested by Letellir et al. [20]

The deposition of cluster Li at higher than 0 V is explainable by a model of "potential barrier between two sites" reported by Zheng et al. [21] The model interprets the hysteresis of the electrochemical potential during charge and discharge in some carbons by supposing the middle of the

potential plateau between charge and discharge to the true potential of a state of doped Li. The potentials of plateau-like regions of cluster Li on discharge curves (broken lines in Fig. 4) were 0.04 ~ 0.10 V, so that the "true" potential of cluster Li is predicted to 0.02 ~ 0.05 V. Therefore, cluster Li can deposit before the charging potential arriving at 0 V. The beginning potentials of Li deposition are evaluated to be 0.004 ～ 0.010 V because the charge volumes of over and under the potentials (shown in Table 3) become comparable values estimated from NMR: the ratios of above / below 0.004 V on (A) (0.26) and above / below 0.010 V on (B) (1.17) corresponded to NMR results.

It is difficult to estimate the distribution of pore-diameter in hard-carbon precisely by the method of N_2 gas adsorption, since adsorbed N_2 molecules diffuse awfully slowly and do not reach to an equilibrium state over a week. However, the pore sizes of sample (A) and (B) are evaluated to be comparable to each other from the NMR spectra (Fig. 6, 7); the shifts of Li cluster below 240 K are practically the same, and only the intensities of the signals are different. Densities of the samples (A) and (B) measured using butanol and helium gas are shown in Table 4. The density of (A) measured by the He gas method was smaller than that of (B), although the butanol method leaded the same density of 1.52 g cm^{-1}. This means that the macroscopic structure of carbon (A) above the size of butanol molecule (≈ 1 nm) is not different from carbon (B), but the microscopic pores of (A), in which only He atom can be adsorbed, are fewer than (B). Because of

comparable sizes of a He atom and a Li ion, a pore not accessible by He atom should be also inaccessible for Li ion. In the novel hard-carbon (A), it is inferred that microporous structure and the diameter of pores are not changed from the present hard-carbon (B), but some pores are closed from outside and Li cannot access to the sites. It may cause the smaller initial irreversible capacity (53 mAh g^{-1}) of the cell using (A), since accessing of Li ion to some of chemically unstable sites in pores are prevented.

The descriptions of pore structure in hard-carbon, which have been suggested, are roughly classified to two: the space surrounded by edges of graphene sheets (based on the Franklin model [4]) and the void spreading between graphene sheets [22] (based on the Conard model [5]). Although the present hard-carbon samples are expected to have both of pore types, the pores not connected from outside are predicted to the type of the former because the latter is easily accessible by Li ion two-dimensionally. The diffusion of Li ion into ink-bottle type of the former can be easily blocked by transformation of the entrance structure. It is inferred that a little modification on the edge structure of novel hard-carbon led the desirable properties for the large size devices.

Conclusion

Four lithium species, Li ion intercalated into graphene sheets, Li ion on the edge of graphene, quasimetallic Li in pore and deposited Li metal, were observed on the charged novel hard-carbon, Carbotron P(J). The small

particles in hard-carbon materials showed different properties from larger particles. The result is especially noticed when making thinner anode of battery used in high charge-discharge rate. The difference between CV capacities on electrochemical evaluation and areas of quasimetallic Li in NMR spectra could be explained by the potential barrier model [21].

Smaller CV capacity and initial irreversible capacity, which is the features of the novel hard-carbon, are considered to be due to a blockade of the diffusion of Li into closed pore area.

Acknowledge

We are grateful to experimental supports of Mr. Shinobu Ohki in National Institute of Material Science, and Prof. Tetsuo Asaji in College of Humanities and Sciences, Nihon University.

References

[1] J. R. Dahn, A. K. Sleigh, H. Shi, B. M. Way, W. J. Weydanz, J. N. Reimers, Q. Zhong, U. von Sacken, in: G. Pistoia (Ed.), Lithium Batteries, New Materials, Developments and Perspectives, Elsevier, Amsterdam, 1994, pp.1-47.

[2] Y. Tanjo, T. Abe, H. Horie, T. Nakagawa, T. Miyamoto, K. Katayama, Soc. Automotive Engineers, SP-1417 (1999) 51-55.

[3] K. Tokumitsu, A. Mabuchi, H. Fujimoto, T. Kasuh, J. Electrochem. Soc., 143 (1996) 2235-2239.

[4] R. E. Franklin, Proc. Roy. Soc., A209 (1951) 196-218.

[5] J. Conard, P. Lauginie, Tanso, 191 (2000) 62-70.

[6] G. M. Jenkins, K. Kawamura, Polymeric Carbons, Cambridge University Press, 1976.

[7] M. Shiraishi, in: Kaitei-Tansozairyonyumon, Carbon Soc. Jpn., Tokyo, 1984, pp.33.

[8] A. Nagai, M. Ishikawa, J. Masuko, N. Sonobe, H. Chuman, T. Iwasaki, Mat. Res. Soc. Symp. Proc., 393 (1995) 339-343.

[9] K. Tatsumi, J. Conard, M. Nakahara, S. Menu, P. Lauginie, Y. Sawada, Z. Ogumi, Chem. Commun., (1997) 687-688.

[10] K. Tatsumi, T. Kawamura, S. Higuchi, T. Hosotubo, H. Nakajima, Y. Sawada, J. Power Sources, 68 (1997) 263-266.

[11] K. Tatsumi, J. Conard, M. Nakahara, S. Menu, P. Lauginie, Y. Sawada, Z. Ogumi, J. Power Sources, 81-82 (1999) 397-400.

[12] S. Wang, H. Matsui, H. Tamamura, Y. Matsumura, T. Yamabe, Phys. Rev., B58 (1998) 8163-8165.

[13] K. Guérin, M. Ménétrier, A. Février-Bouvier, S. Flandrois, B. Simon, P. Biensan, Solid State Ionics, 127 (2000) 187-198.

[14] S. Yamazaki, T. Hashimoto, T. Iriyama, Y. Mori, H. Shiroki, N. Tamura, J. Mol. Struct., 441 (1998) 165-171.

[15] S. Gautier, F. Leroux, E. Frackowiak, A. M. Faugére, J.-N. Rouzaud, F. Béguin, J. Phys. Chem. A, 105 (2001) 5794-5800.

[16] Y. Ohashi, Y. Shigaki, Eur. Pat. Appl. (1996) EP 726606.

[17] K. Shimizu, M. Maeda, S. Morinishi, A. Nagai, A. Hoshi, PCT Int. Appl. (2005) WO 2005098999.

[18] P. Scherrer, Nachr. Ges. Wiss. Göttingen, 2 (1918) 98.

[19] G. C. Carter, L. H. Bennet, D. J. Kahan, in: Metallic Shifts in NMR, Part I, Pergamon Oxford, 1977, pp. 239.

[20] M. Letellier, F. Chevallir, F. Béguin, E. Frackowiak, J. -N. Rouzaud, J. Phys. Chem. Solids, 65 (2004) 245-251.

[21] T. Zheng, W. R. McKinnon, J. R. Dahn, J. Electrochem. Soc., 143 (1996) 2137-2145.

[22] M. Nagao, C. Pitteloud, T. Kamiyama, T. Otomo, K. Itoh, T. Fukunaga, K. Tatsumi, R. Kanno, J. Electrochem. Soc., 153 (2006) A914-A919.

Figure Captions

Fig. 1.

The scanning electron micrograph of the carbon (A).

Fig. 2

Powder XRD patterns of carbon (A), (B) and (C).

Fig. 3.

Particle-size distributions of sample (A) (◆),(B) (○), (C) (□) and sieved sample (D) (+). (A) and (B) have almost the same distributions. The mean-sizes of (A), (B) and (C) are shown in Table 1.

Fig. 4.

Charge (lithiation process: solid line) and discharge (lithium extraction process: broken line) curves of the sample (A), (B), (C).

Fig. 5.

Room-temperature ^{7}Li MAS NMR spectra of sample (A) at 0.1 V (155 mAh g^{-1}), 0.0 V (300 mAh g^{-1}) and 0.0 V (500 mAh g^{-1}). Peaks checked by symbol (∗) are spinning side bands.

Fig. 6.

Temperature dependence of static ^{7}Li NMR spectrum on fully charged sample (A).

Fig. 7.

Temperature dependence of static ^{7}Li NMR spectrum on fully charged sample (B).

Fig. 8.

Temperature dependence of static ^{7}Li NMR spectrum on fully charged sample (C).

Fig. 9.

Room-temperature ^{7}Li MAS NMR spectra of fully-charged sample (B) and refined sample (D) made by sieving and cutting off over 5 μm particles of (B). Peaks checked by symbol (∗) are spinning side bands.

Fig. 10.

The deconvolution of static ^{7}Li NMR spectra at 180 K for (a): sample (A), and (b): sample (B).

Tables

Table 1 The interlayer distances (d_{002}), the crystallite size factors (Lc_{002}) calculated from XRD(002) reflection using Scherrer formula [18], and the mean particle-sizes of three carbon samples.

sample	d_{002} / nm	L_{C002} / nm	particle size / μm
(A)	0.374	1.40	9
(B)	0.379	1.31	9
(C)	0.380	1.10	22

Table 2 The results of electrochemical evaluation of cells using samples (A) ~ (C).

sample	whole charge capacity / mAh g^{-1}	CC capacity / mAh g^{-1}	CV capacity / mAh g^{-1}	initial irreversible capacity / mAh g^{-1}
(A)	352	305	47	53
(B)	530	264	266	77
(C)	511	240	271	73

Table 3 The capacities and the ratios above / below 0.004 V and 0.010 V of (A) and (B) read from the charge curves in Fig. 2.

sample	whole charge capacity / mAh g^{-1}	capacity above / below 0.004 V / mAh g^{-1}	ratio of above / below 0.004 V	capacity above / below 0.010 V / mAh g^{-1}	ratio of above / below 0.010V
(A)	352	72 / 280	0.26	96 / 256	0.37
(B)	530	274 / 256	1.07	286 / 244	1.17

Table 4 The densities measured by butanol liquid and helium gas.

sample	butanol	helium
(A)	1.52	1.96
(B)	1.52	2.08

Fig 1

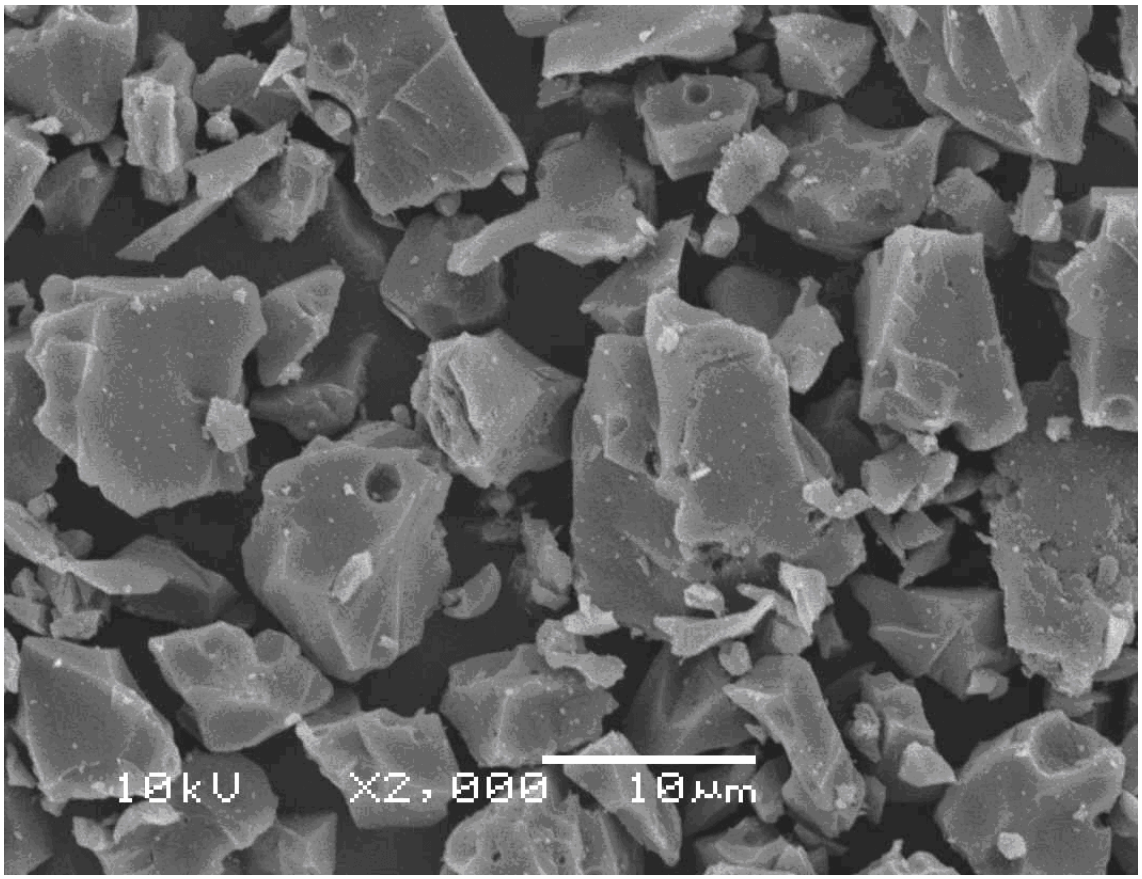

Fig 2

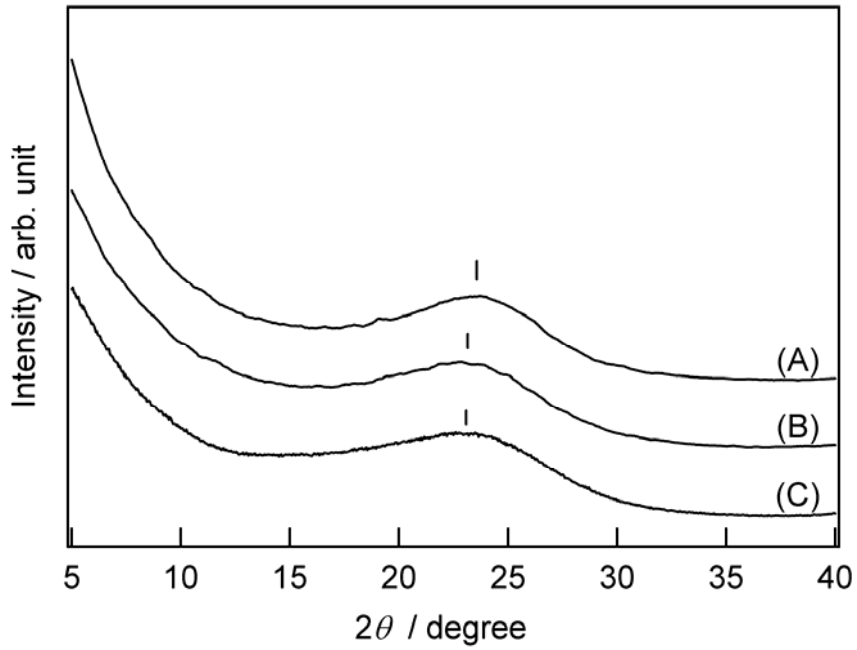
Intensity / arb. unit
(A)
(B)
(C)
5
10
15
20
25
30
35
40
2θ / degree

Fig 3

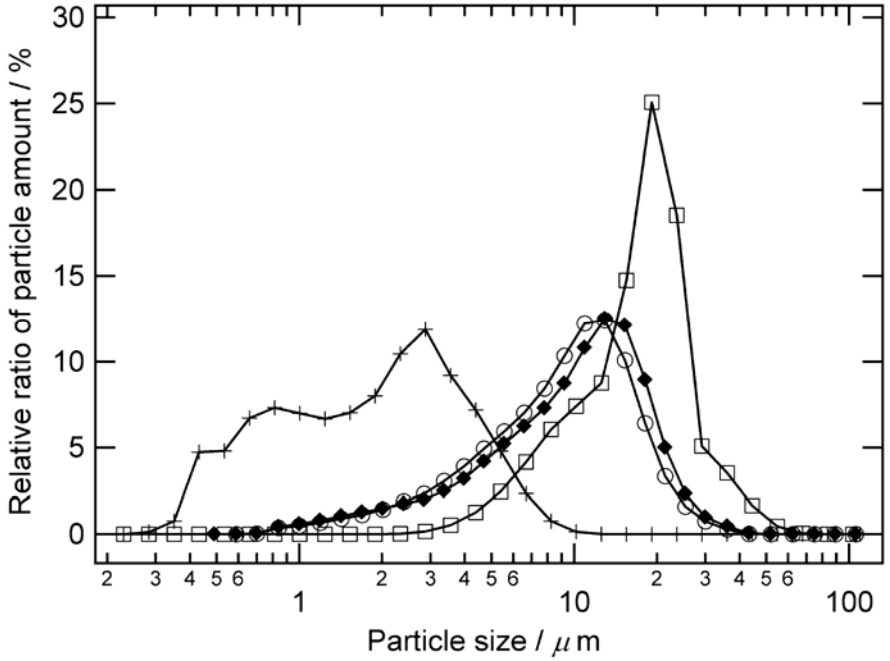
Relative ratio of particle amount / %
30
25
20
15
10
5
0
2 3 4 5 6
1
2 3 4 5 6
10
2 3 4 5 6
100
Particle size / μm

Fig 4

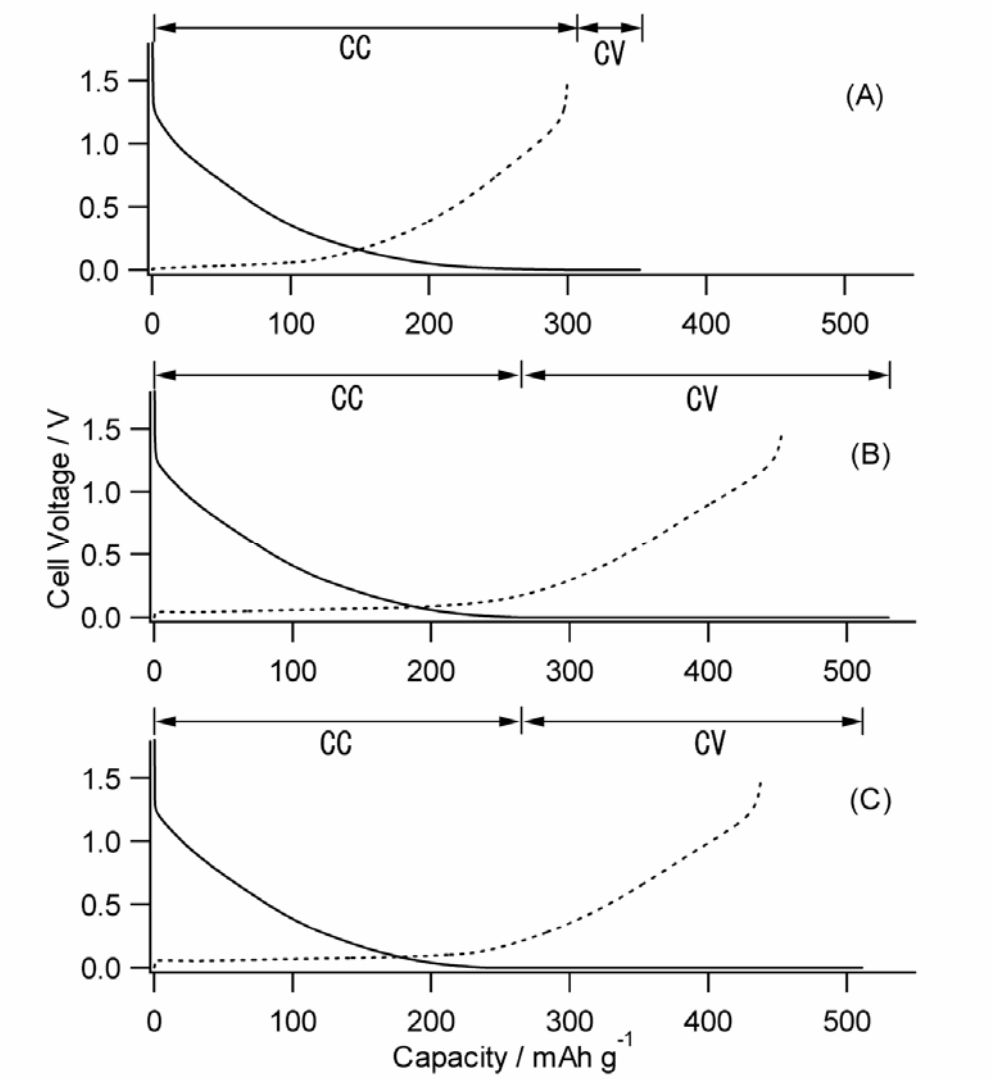
CC
CV
(A)
(B)
(C)
Cell Voltage / V
Capacity / mAh g-1
0.0
0.5
1.0
1.5
0
100
200
300
400
500

Fig 5

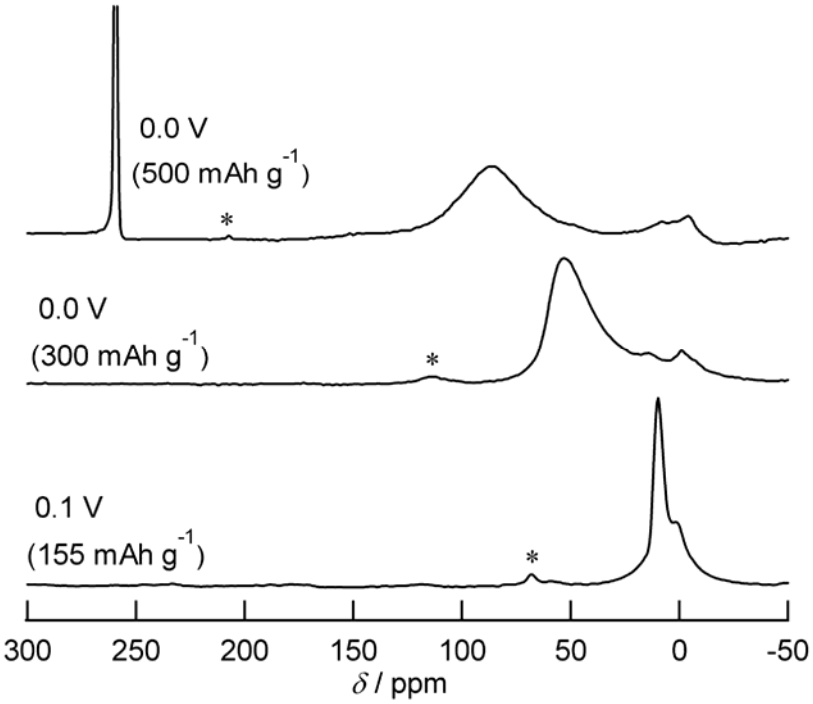
0.0 V
(500 mAh g-1)
*
0.0 V
(300 mAh g-1)
*
0.1 V
(155 mAh g-1)
*
300
250
200
150
100
50
0
-50
δ / ppm

Fig 6

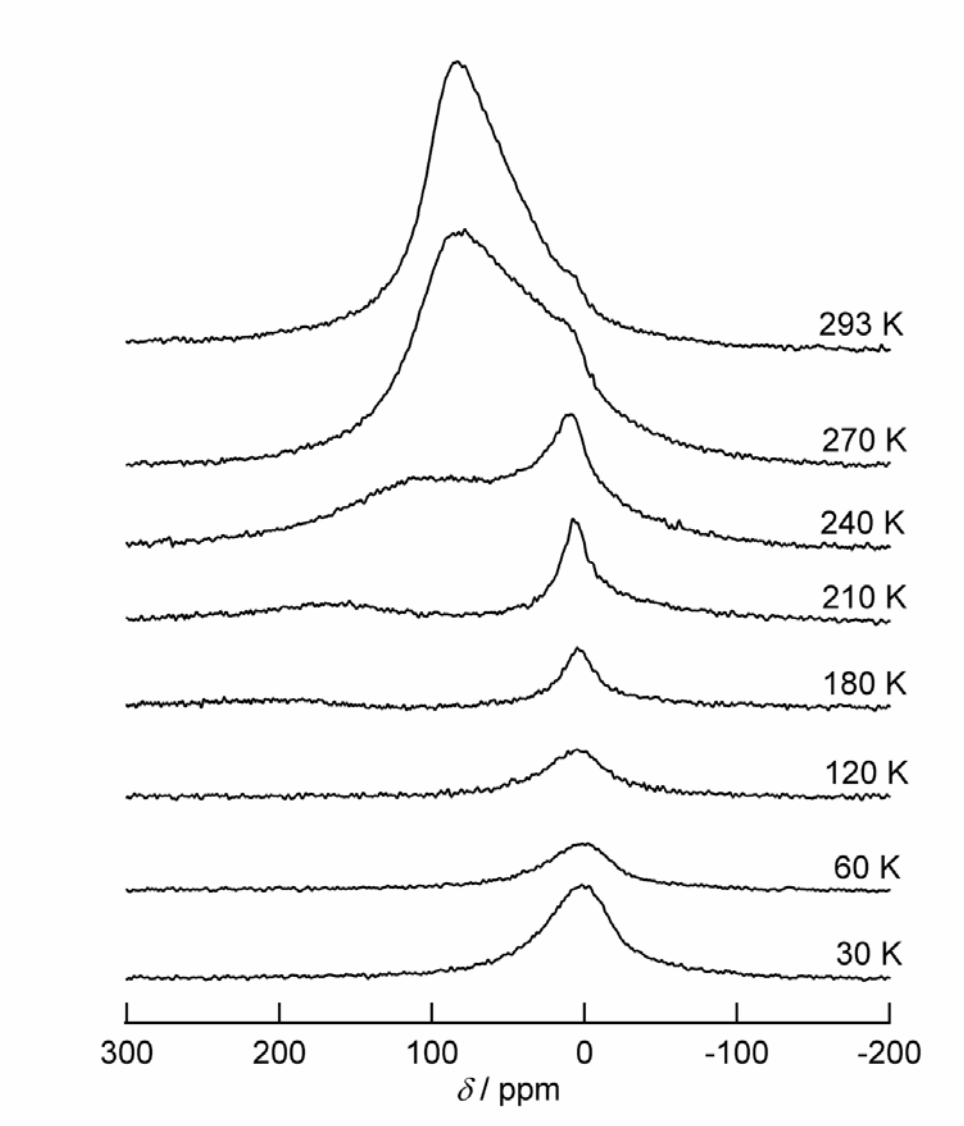
293 K
270 K
240 K
210 K
180 K
120 K
60 K
30 K
300
200
100
0
-100
-200
δ / ppm

Fig 7

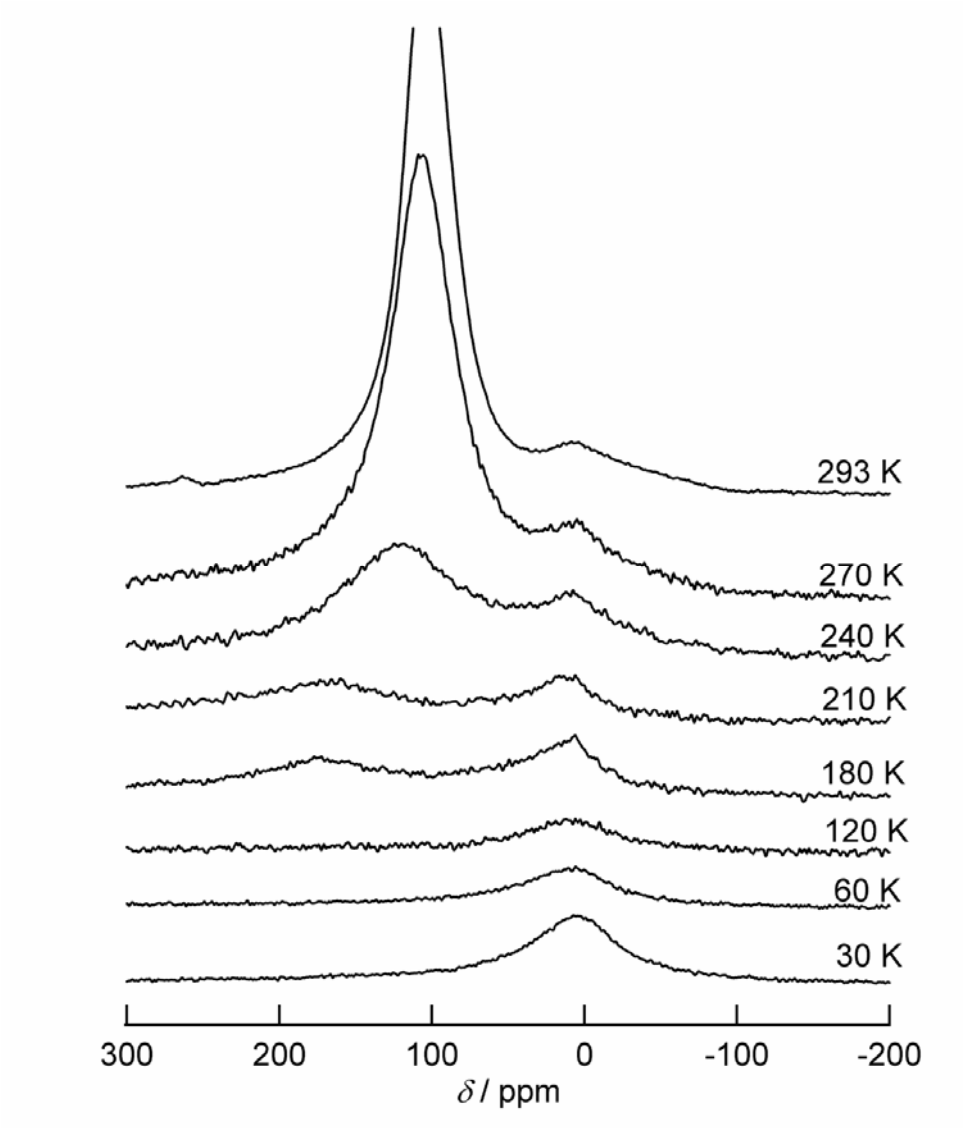
293 K
270 K
240 K
210 K
180 K
120 K
60 K
30 K
300
200
100
0
-100
-200
δ / ppm

Fig 8

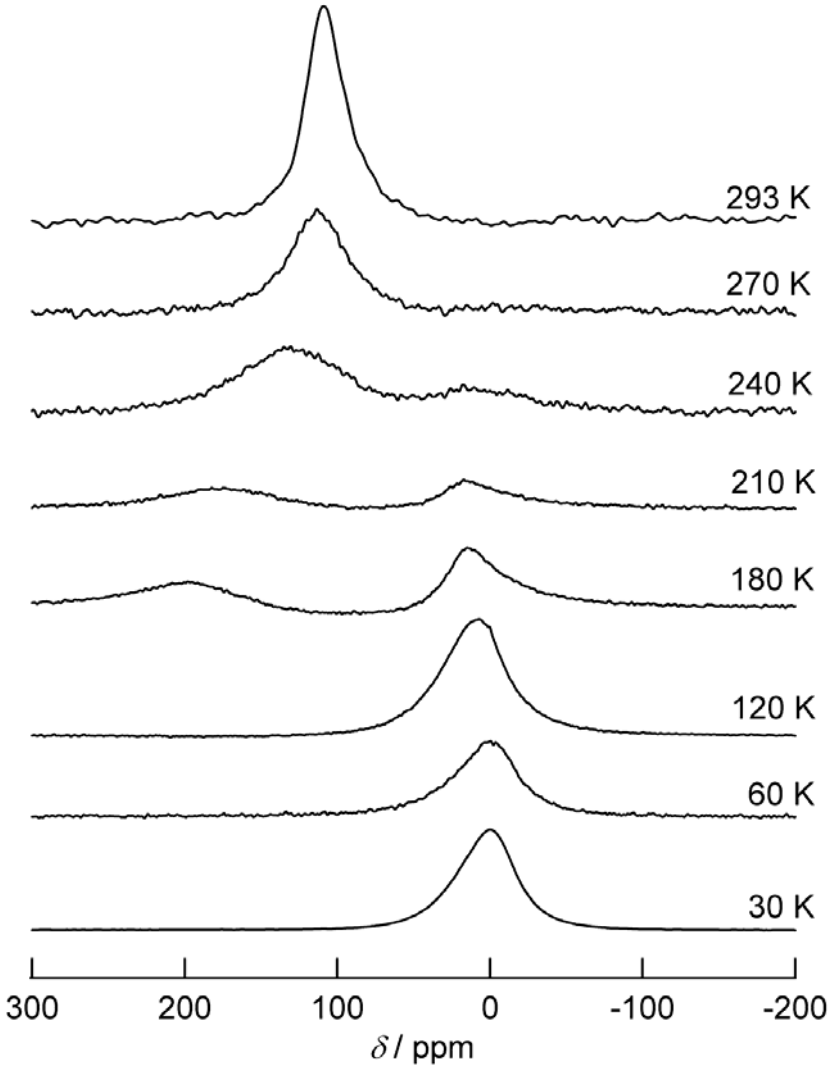
293 K
270 K
240 K
210 K
180 K
120 K
60 K
30 K
300
200
100
0
-100
-200
δ / ppm

Fig 9

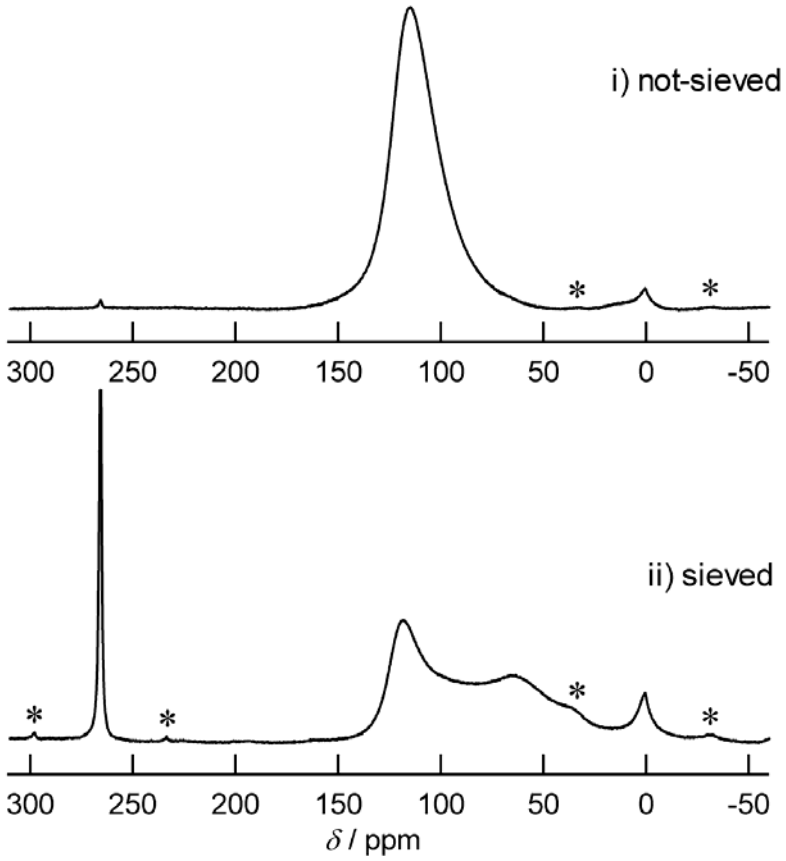

Fig 10a

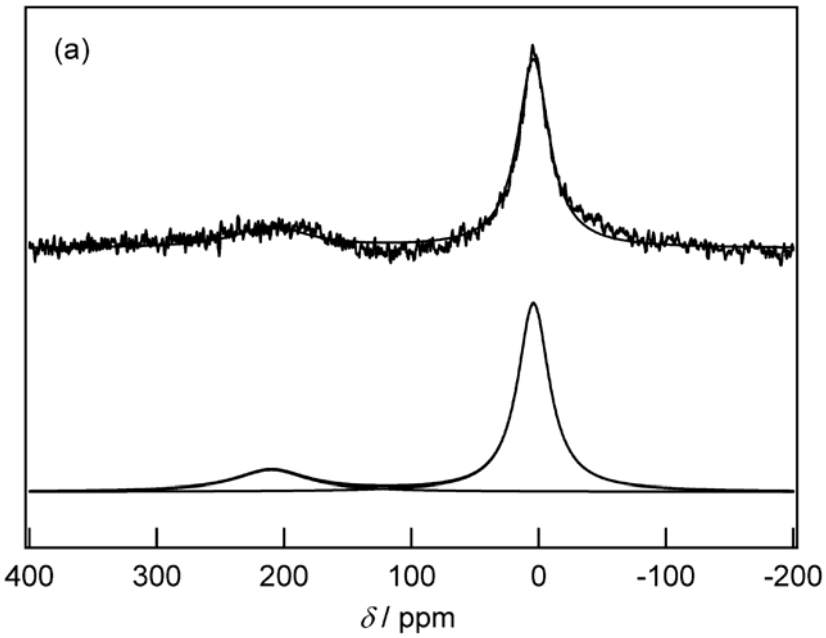

Fig 10b